Reproductive Sciences (2023) 30:2401–2415
https://doi.org/10.1007/s43032-023-01200-4

ORIGINAL ARTICLE

Oxidative Stress and Cell Cycle Arrest in Seminiferous Tubules Nearby Varicose Vessels: New Perspectives from Experimental Varicocele

Aram Minas[1] · Mazdak Razi[2] · Mohammad Hossein Nasr-Esfahani[3] · Seyed Mohammad Hashemi-Asl[4] · Marziyeh Tavalaee[3]

Received: 8 November 2022 / Accepted: 8 February 2023 / Published online: 23 February 2023

Abstract

Varicocele (VCL) has been shown to induce severe oxidative stress in the testicular tissue resulting in 35% of males with primary infertility. To compare the exacerbating impacts of varicose on oxidative DNA damage and homeostatic antioxidant reactions in the seminiferous tubules (ST), enclosed and far from varicose vessels. Thirty mature *Wistar* rats were divided into control and VCL-induced groups. To approve VCL, the testicular diameters, volume, and blood circulation were measured using B-mode and Doppler ultrasonography. Next, to confirm oxidative stress (OS), the global homeostatic antioxidant biomarkers were evaluated. Moreover, the OS-induced oxidative DNA damage and homeostatic antioxidant reactions were compared between STs nearby and far from varicose vessels. Finally, to clarify the DNA damage-induced impact on the cell cycle progression, the global and local expressions of Cyclin D1, Cdk4, and p21 were examined. The VCL-induced group exhibited diminished global antioxidant status (marked with TAC, GPX, SOD, and CAT) and UNG and MPG expression levels. Moreover, the cross-sections of the VCL group represented a prominent reduction in the UNG, MPG, Cyclin D1, and cdk4, and upregulation in the p21 expression levels, more prominently in the STs nearby varicose vessels. Concerning severe oxidative DNA damage and intensive molecular changes in the STs nearby the varicose vessels, they can be considered the main cause of oxidative DNA damage in enclosed tubules. Thus, the varicose-mediated oxidative DNA damage negatively impacts the cell cycle progression in the tubules more intensively in the subcapsular area.

Keywords Varicocele · Varicose vessels · Oxidative stress · DNA repairmen · Cell cycle

Introduction

During the last decades, infertility has become a public health issue, affecting more than 15% of couples during their reproductive age [1, 2]. Accordingly, 40–50% of infertilities are attributed to male infertility problems [2–4]. Among various male infertility disorders, the varicocele (VCL) has been highlighted according to its high incidence of 35% in males with primary infertility. However, it dramatically increases to more than 80% in men with secondary infertility [5, 6]. Concerning the complexity of the left-sided vasculature and a vertical entrance of blood to the renal vein at the right angle, the left-sided VCL is more common (80%) in men [7]. Thus, the VCL is determined by a pathological enlargement of the pampiniform plexus with twisted veins, caused by the turbulent blood flow and reverses pressure, leading to a retrograde blood flow-down, usually from the left spermatic vein [8]. Moreover, as another etiology of VCL, the absence and/or incomplete formation of valves in the left testicular vein, mainly at the pelvic and lumbar sites, is reported in 33–37% of patients [9]. Several experimental and clinical studies have shown the VCL-related pathophysiology in testicular tissue, including decreased testicular endocrine status [10], heat [11], oxidative, nitrosative [12–14], and endoplasmic reticulum-related [15] stresses

✉ Mazdak Razi
Mazdak.razi@gmail.com

1 Department of Surgery, Division of Urology, Human Reproduction Section, Universidade Federal de São Paulo-UNIFESP, São Paulo, Brazil

2 Department of Basic Science, Faculty of Veterinary Medicine, Urmia University, Urmia, Iran

3 Department of Animal Biotechnology, Jahad Daneshgahi Biotechnology Research Institute, Royan Research Institute, Reproductive Medical Research Center, Isfahan, Iran

4 Department of Surgery and Diagnostic Imaging, Faculty of Veterinary Medicine, Urmia University, Urmia, Iran

as well as inflammation [16]. The VCL-induced oxidative stress (OS), due to its suppressive effects on the testicular antioxidant capacity [17], has been highlighted by different experimental and clinical trial studies, representing its deleterious effect on DNA, mRNA [18–20], lipids, and protein contents [19, 21, 22].

Cyclins, with 20 members in the family, are the most known cell cycle regulators, which coordinate with their special kinases (Cdks) in maintaining cell cycle machinery [23, 24]. Accordingly, pathological suppression of Cyclins and Cdks expression and/or a disrupted Cyclins/Cdks complex formation inhibits the cell cycle progression by inducing cell division arrest [23, 25, 26]. The Cyclin D1, a member of the D family, in response to DNA damage under OS condition, controls the G1/S stages during the cell cycle [27] by switching the pathway in developing germ cells to the DNA repairmen process and/or apoptosis [28] through p21 and p53 proteins mediation [23]. The current signaling is revealed in the experimental VCL condition using rats, showing a diminished Cyclin D1 expression simultaneous with massive oxidative DNA damage as well as increased p21 expression in the testicles [19, 29]. Indeed, the p21 (WAF1, CAP20, Cip1, and Sdi1), another critical cell cycle regulator after oxidative DNA damage, stops the cell cycle development by restricting cdk4 to block cdk4/Cyclin D1 complex formation [23, 30]. Therefore, it can be concluded that the p21 and Cyclin D1-induced role has a role in mediating the severe oxidative DNA damage in the VCL condition.

As a central DNA repair process in the testicular tissue, the "Base Excision Repair (BER)" pathway plays an undeniable role in removing the DNA lesions in various circumstances such as OS [31]. The BER pathway is divided into different stages, including detection and cutting, incision, replacement, processing of DNA terminals, and sealing the DNA [32]. The DNA glycosylases carry out the cognition and excision of DNA lesions, which is an essential process to initiate the BER pathway. With respect to their specificity, each DNA glycosylase plays a particular role in the DNA repair process. For instance, uracil-DNA glycosylase (UNG) removes Uracil (U) DNA lesions raised from deamination of the cytosine or U misplace during DNA synthesis [33], while methylpurine DNA glycosylase (MPG), detects, removes, and ultimately repairs the DNA alkylated bases [34]. Thus, any disruption in the UNG and MPG-related interactions can significantly affect the DNA repairing machinery and enhance the mutatic legions transfer to the next generation.

Considering an expanded VCL-induced varicose formation in the vasculature network of testicles [10, 35] and the possible boosting effect of varicose on the OS induction [36], we divided the testicular cross-sections into two subcapsular and central zones, and investigated the changes in those seminiferous tubules around varicoses by comparing them to those with more distance. Consistent with this issue, first, the VCL-induced OS and DNA damage biomarkers, as well as histopathological changes in the testis, were aimed to be investigated. Second, the VCL-induced DNA damage impact on cell cycle machinery, especially Cyclin D1/p21 cooperation, was targeted. Finally, DNA repair enzyme activity, majorly focusing on the UNG and MPG enzymes (those playing a pivotal role in the DNA repairing system), and germ cell survival were investigated.

Method and Material

Chemicals

To perform the immunohistochemistry (IHC) staining, the primary antibodies for anti-UNG (Cat NO: E-AB-66016), anti-MPG (Elabsciences, USA, Cat NO: E-AB-60952), anti-8-Oxo-G (Elabsciences, USA, Cat No: E-AB-52306), anti-cyclin D1 (Elabsciences, USA, Cat No: E-AB-64003), Cdk-4 (Elabsciences, USA, Cat No: E-AB-52141), and anti-p21 (Elabsciences, USA, Cat No: E-AB-70068) were purchased from ElabSciences company branch in Turkey (Istanbul, Turkey). Additionally, Horseradish peroxidase-labeled avidin–biotin complex ("HRP," VectorLabs, Peterborough, UK) was assigned from Life-TebGen CO, (Tehran, Iran). The commercial kites for glutathione peroxidase (GPX, Cat N: NS-15087), superoxide dismutase (SOD, Cat N: NS-15032), catalase (CAT, Cat N: NS-15052), and total antioxidant capacity (TAC, Cat N: NS-15012) were purchased from Navand Salamat Company (Navand Salamat Co. Urmia, Iran). TUNEL (terminal deoxynucleotidyl transferase enzyme-mediated dUTP nick end labeling) assay kit (Roche, Cat NO: 11684817910, Germany) was purchased Setareye Pajohesh Asia Co. Other materials were standard commercial laboratory chemicals.

Animals and Groupings

To perform the current experimental original study, 30 mature male Wistar rats (150 ± 20 g) were purchased from a laboratory animal house, Faculty of Veterinary Medicine, Urmia University. The animals were subdivided into the Control (No = 15) and experimental VCL-induced (No = 15) groups following two weeks of adaptation. During the experimental period (4 months), all rats were kept in a standard condition by minimizing stress factors and ad libitum access to food (rat pellet) and water, based on the guidelines of Urmia University for research using animal models. All experimental protocols were evaluated and approved by the Faculty of Veterinary medicine's ethical committee, Urmia University (Ethical Number: IR-UU-AEC-1779/DA/3). No surgical intervention was applied to the control group.

VCL Induction

The experimental VCL was applied based on Turner's method by partially ligating the left renal vein near the caudal vena cava [37]. To induce deep anesthesia, after weighing the rats, an appropriate dose of ketamine (10 mg/kg) and xylazine (5 mg/kg, Alfasan, Woerden, The Netherland) were injected intraperitoneally, the abdominal midline was shaved, scrubbed, and an incision (3–5 cm) was applied on the midline. Next, the anatomical joining of spermatic and renal veins was identified and partially ligated by a 4–0 silk suture, which was previously tied around 0.8 mm round needle and renal vein before removal. Finally, the left spermatic vein's expansion was rechecked, and the abdominal midline incision was closed by suturing the muscular and skin layers.

Ultrasonography Examination

At the end of the study (day 120), the testicular and vein diameters, blood flow pattern, and blood dynamicity of the testicular tissue (left and right testicles of the control and VCL induced animals) were examined by a Q9vet ultrasound machine (Chison Medical Imaging CO., LTD.) with a 10 MHz linear transducer (D7L40L), after general anesthesia. A systematic examination of the longitudinal and transverse planes and length, width, and height of each testis were examined by two-dimensional gray-scale ultrasonography, as previously described by al Kwon et al. [38]. The subcapsular vessels and veins and testicular parenchymal blood flow patterns, as well as pulls wave (PW), were examined by mid-sagittal plan Doppler ultrasonography with color mode.

Tissue Sampling

Subsequently, after sonography examination, the rats were euthanized by intraperitoneal ketamine and xylazine cocktail administration, and after weighing, the left testicular tissue was aseptically dissected out and weighed, as well. Then, the tissues were divided into half; one to store at − 70 °C for biochemical and RT-PCR analyses, and the other to fix in the formalin fixative solution (10%) for histopathological and IHC staining.

Biochemistry Examination

To approve the OS condition in the testicles, the enzymatic antioxidant status and the total antioxidant capacity (TAC) of the testicular tissue, as well as immunoreactivity of 8-oxodG (see next), were analyzed. For biochemical analyses, 20–30 mg of the tissue was homogenized in 1000 µl of lysis buffer, centrifuged (9000 rpm, 15 min), and the supernatant was collected. For the CAT activity of testicular tissue, the reaction was performed in 300 µl containing 60 µl of supernatant and 240 µl from different reagents of the kit. After all stages of the test (according to the manufacturer's instructions), the absorbance was immediately monitored at 550 nm. The CAT activity was calculated based on the formula ($y = 0.0087x + 0.3244$, $R^2 = 0.96$) obtained from standards ODs and concentrations. The results are expressed as U/mg protein (CAT, Cat N: NS-15052, Navand Salamat Co. Urmia, Iran). For testicular GPX, the reaction was performed in 300 µl containing 40 µl of supernatant and 260 µl from different kit reagents. After all stages of the test (according to the manufacturer's instructions), the absorbance was monitored at 340 nm, with two intervals of 5 min. The GPX activity was calculated based on the formula ($y = 0.0083x + 0.06$, $R^2 = 0.98$) obtained from standards ODs and concentrations for NADPH concentration, continued to obtain GPX activity by using a formula based on NADPH concentration/ (ΔODs × sample volume) × dilution. The results are expressed as nmol/min/ml (GPX, Cat N: NS-15087, Navand Salamat Co. Urmia, Iran). For testicular SOD, the reaction was performed in 300 µl containing 50 µl of supernatant and 250 µl from different reagents of kit. After all stages of the test (according to the instructions of the manufacturer), the absorbance was immediately monitored at 405 nm. The SOD activity was calculated on the basis of the formula (OD of sample/OD of control). The results are expressed as U/mg protein (SOD, Cat N: NS-15032, Navand Salamat Co. Urmia, Iran). The total protein contents of samples were evaluated based on Lowry's method [39]. For testicular TAC, the reaction was performed in 1000 µl reaction buffer containing 100 µl supernatant, 400 µl distilled water, 500 µl $ABTS^+$ buffer (containing 100 µl ABTS + 800 µl distilled water + 100 µl potassium persulfate (10 ×) with the absorbance of 1.14). After incubation at room temperature (5 min), the absorbance was monitored at 414 nm. The TAC level was calculated on the basis of the formula ($y = -0.007x + 0.6505$, $R^2 = 0.98$) obtained from standards ODs and concentrations. The results are expressed as nmol/mg protein (TAC, Cat N: NS-15012, Navand Salamat Co. Urmia, Iran).

Histological Assessment

The fixated samples were routinely passaged in ascending alcohols (70%, 80%, 90%, and 98%), embedded, and cut (5–6 µm) by automatic rotary microtome (Historage, 2218, UK). The tissue sections were stained (Hematoxylin and Eosin staining, H&E) and prepared for histomorphometric evaluation. To approve the sonography results, the presence of varicose in the microvasculature's of subcapsular and central zones was analyzed by evaluating the vascular diameter (compared to those in the control group). Moreover, to confirm the VCL condition, the edema in the interstitial connective tissue, spermiogenesis index (SPI, the

seminiferous tubules with active spermiogenesis), Johnsen's score (Table 1), the height of germinal epithelium, tubular diameter, and general histological changes were analyzed as previously described [10, 16]. All histomorphometric data were compared between the central and subcapsular zones.

Immunohistochemistry (IHC)

To analyze the effect of VCL on the BER enzymes (UNG and MPG) as well as proteins involving in the cell cycle process (Cyclin D1, cdk4, and p21), and to compare the changes in the pattern of protein expression between subcapsular and central zones, the IHC staining was considered. The histological sections were cut and placed at 56 °C in a hot air oven (Venticell, MMM, Einrichtungen, Germany) for 25 min. Next, the samples were de-paraffinized in xylene (2×) and subsequently rehydrated through a series of graded alcohol concentrations (99%, 90%, 80%, 70%; each for 5 min). The antigen retrieval process was conducted by incubating the slides in a ten mM sodium citrate buffer (pH: 7.2), using a microwave device (720w for 3 min and 150 w 11 min). The endogenous peroxidases were blocked using 1.5% hydrogen peroxide in 1×phosphate buffer (PBS, 20 min at room temperature). After washing (3 min in 1×PBS), the slides were incubated in a superblock solution (SCYTEK Co, AA025, Utah, United States of America, LOT:43,961) for 10 min. The control (no primary antibody) and experimental slides were incubated overnight at 4 °C, respectively, with the blocking solution alone or blocking solution with UNG (1:400), MPG (1:350), Cyclin D1 (1:300), cdk4 (1:350), and p21 (1:300). Subsequently, the slides were washed with 1×PBS and incubated with peroxidase/HRP conjugated Goat Anti-Rabbit IgG secondary antibody (1:500, Elabscienece, USA, Cat N: E-AB1003) for 60 min at room temperature. Finally, the slides were incubated with a standard 3,3′-Diaminobenzidine chromogen solution (DAB; Sigma, St. Louis MO) (5 min) to visualize the labeled proteins and then counterstained with hematoxylin (10 s). The MPG^+, UNG^+, Cyclin $D1^+$, $cdk4^+$, and $p21^+$ cells were counted *per* seminiferous tubules with the same criteria located near the varicose vessels subcapsular and central zones and compared between groups. Moreover, the pixel-based intensity of brown reactions, representing the labeled proteins in the germ cells, was assessed by software (Image J software, National Institutes of Health, USA) in the seminiferous tubules with the same criteria at 2530 µm × 2530 µm of a cross-section from each animal. For this purpose, 20-megapixel images were prepared by the onboard camera (Zeiss, Cyber-Shot, Japan) and then, the mean of pixel-based intensities, obtained form 3 images from cross-sections of each animal (in total 45 cross-sections/each group), were evaluated, and finally, the mean ± SD of intensities was compared between groups.

Table 1 Grading based on Johnsen's score

Condition	Score
No germ cells or Sertoli cells present	1
No germ cells present	2
Only spermatogonia present	3
Only a few spermatocytes present	4
No spermatozoa or spermatids present but many spermatocytes present	5
Only a few spermatids present	6
No spermatozoa but many spermatids present	7
Only a few spermatozoa present	8
Many spermatozoa present but disorganized spermatogenesis	9
Complete spermatogenesis	10

TUNEL Staining and Apoptosis Index

To assess the effect of VCL on apoptosis index, the TUENL staining was conducted using a commercial in situ cell death detection kit (Roche, Germany, UNSPSC Code: 12,352,200). The slides were prepared and rehydrated as previously described for IHC staining. The digestion step was initiated using an appropriate concentration of proteinase K (10–20 µg mL^{-1} in 10 mM Tris/HCL, pH 7.4–8) for 15 min. The slides were washed with 1×PBS (3×) and incubated (1 h) in the TUNEL solution (prepared as the manufacturing company recommended). After washing with 1×PBS (3×), the slides were incubated in the POD-convertor (30 min), and after that, covered with DAB solution (60 s). Subsequently, the slides were counterstained with hematoxylin. Finally, the apoptotic index was assessed [40] and compared between the testicular cross-section subcapsular and central zones. Moreover, similar to IHC slides, the pixel-based intensity of brown reactions (representing apoptosis) was analyzed in a 2350 µm × 2350 µm of tissue.

Immunofluorescence Staining of 8-oxodG in Testicular Tissue

Frozen slides (8–10 µm) were prepared and immersed in chilled PBS (5 min). The nonspecific binding sites were blocked using ready to use superblock (Scytek laboratories, USA, REF N:AAA025) solution (30 min). Then, the cross-sections were incubated overnight with the primary antibody specific for 8-oxodG (Genox Corporation, USA, Code N: MOG-020P diluted 1:100), at 4 °C. The blocking serum alone was considered for the control section. The sections were washed in PBS and incubated with fluorescent anti-mouse secondary antibody (IgG) conjugated to Alexa Fluor® 594 (Abcam, Uk, Cat N: ab150120) for 30 min at

room temperature. The cross-sections counterstained with 4′,6-diamidino-2-phenylindole (DAPI) to stain nuclear DNA in blue.

RNA Isolation, cDNA Synthesis, and qRT-PCR

The total mRNA content of samples was extracted using TRIZOL-solution-based method [10], and the concentration and quality of the extracted mRNA were analyzed at 260 nm and 260/280 = 1.8–2.0. The total mRNA content of 1 µg was used to synthesize the cDNA. For this purpose, a 20 µl reaction mixture containing 1 µl oligo (dT) primer, 4 µl of 5 × reaction buffer, 1 µl of RNAse inhibitor, 2 µl of dNTP mix (10 mM), 1 µl of M-MuLVReverse Transcriptase, and stabilized RNA with distilled water according to the manufacturer's protocol (Pars tous, Iran) was prepared. To run a real-time PCR reaction, cDNA templates (0.5 µl containing 5–10 ng cDNA), 1X SYBR GREEN master mix (10 µl; High ROX, Noavaran Teb-Beinolmelal, Iran), 0.6 µl of reverse, and 0.6 µl forward primers of each targeted genes were mixed with sufficient distilled water (the whole mixture was 20 µl). The PCR condition was set as 95 °C (600 s), 95 °C (20 s), and 72 °C (60 s) for denaturation (one cycle), annealing and elongation (45 cycles) stages, respectively. Finally, one cycle (600 s at 72 °C) was considered for the elongation. The sequences of the primers are presented in Table 2. Each sample had three repetitions, and analysis was normalized with the GAPDH threshold cycle (CT) values. The fold change was calculated by the equation: $2^{-(\text{Ct target} - \text{Ct GAPDH})}$.

Photography, Imaging, and Design

The fluorescent photomicrographs (8-oxo-dG) were prepared using a fluorescent microscope (Nikon, Japan), equipped with an optical-sectioning device and on-board camera (SONY, Zeiss, Cyber-Shot, Japan). Two different filters, DsRed (Ex 538–562 nm, Em 570–640 nm) and DAPI (Ex 335–383 nm, Em 420–470), were considered in analyzing and imaging the fluorescent-stained slides. The Adobe Photoshop CC software (Version 2018) was used to present the result section's images. Moreover, light microscopy photomicrographs were captured by a SONY on-board camera (Zeiss, Cyber-Shot, Japan).

Statistical Analysis

Kolmogorov–Smirnov and Levene's tests were used to test the results normality and homogeneity, respectively. All quantitative results regarding the ultrasonography, histopathology, and molecular findings were statistically analyzed using one way ANOVA with appropriate post hoc (Turkey's multiple comparison test) and Bartlett's tests. The SPSS software (version 11.00, California, USA) was used to test the correlation and regression between data. Finally, the p-value ($p < 0.05$) was considered a value for statistically significant differences and all data were presented as mean ± SD.

Results

Confirmation of VCL in the Testicular Tissue

First of all, we found a remarkable failure in the testicular blood circulation representing a remarkable varicose generation in the subcapsular and central microvasculature at Doppler ultrasonography examination before euthanizing the rats. Moreover, the VCL-induced rats showed a significant reduction in the testicular sizes (Table 3) and testicular weight relative to total body weight compared to the control group (Fig. 1A–E). To approve the varicose and appropriate VCL induction in rats, the previously showed histological phenotypes [10, 21] in the experimental VCL-induced testicles were rechecked histologically. We demonstrated expanded varicose in the capsular, sub-capsular, and central microvasculature (Fig. 2A, 2B), intensive edema in the connective tissue (Fig. 2C), increased vascular diameter (Fig. 2D), deformed and atrophied seminiferous tubules, an increased percentage of seminiferous tubules with germ cell dissociation (Fig. 2E), and a significant reduction in the germinal epithelium height (Fig. 2F). All mentioned histological alterations were revealed in both sub-capsular and central areas, while the changes were found more evident in the sub-capsular area compared to the central zone. In contrast, no histopathological changes were demonstrated in the cross-sections of the control group. To make these findings more precise, the potency of seminiferous tubules in progressing germ cell differentiation and

Table 2 The primers nucleotide sequences and annulling temperatures used in qRT-PCR

Primer	5′-forward-3′	5′-reverse-3′	Annulling T	Size
MPG	CATTTCTGGGACAGGTTCTTGTC	TGCCTCAGTCTCCACAATGC	47 °C	152
UNG	CAGTGTCCAAAGACCAGTTCCA	AGGATGAACAAAACCATCGATGT	45 °C	212
GAPH	CTGCACCACCAACTGCTT	GCCATCCACAGTCTTCTG	58 °C	185

Table 3 Ultrasonography results

	Right testis					Left testis					
	Width	Length	Height	Volume	V.D	Width	Length	Height	Volume	V.D	Flow
Control 1	1.25	1.83	1.05	1.26	0.08	1.28	1.84	1.06	1.31	0.1	10.27
Control 2	1.17	2.35	1.28	1.84	0.1	1.11	2.38	1.09	1.51	0.12	7.38
Control 3	0.99	2.06	0.95	1.01	0.05	1.06	2.1	1.06	1.24	0.08	7.31
Control 4	1.03	1.85	0.96	0.95	0.05	1.19	1.87	0.96	1.12	0.07	5.59
Control 5	1.14	2.1	1.2	1.40	0.09	1.2	1.95	1.14	1.4	0.09	9.38
VCL 1	1.11	1.93	1.16	1.3	0.1	0.92	1.97	0.99	0.94	0.17	1.01
VCL 2	0.95	1.48	1.28	0.94	0.12	0.95	1.42	0.8	0.57	0.14	1.7
VCL 3	0.94	1.99	0.96	0.94	0.09	0.93	1.27	1.11	0.69	0.13	1.49
VCL 4	1.26	1.95	1.17	1.51	0.14	0.99	2.17	1.01	1.14	0.15	1.97
VCL 5	0.94	2.06	1.28	1.3	0.11	1.04	2.35	0.95	1.22	0.17	2.49

According difference in left and right testicular blood flow, the blood flow was evaluated in left testicular tissue. *V.D*, vascular diameters. All the results are presented in centimeter (cm)

spermiogenesis was assessed by analyzing the percentage of tubules with positive TDI and SPI (in both central and sub-capsular portions) as well as evaluating the general Johnsen's score in a cross-section. Similar to other findings, a remarkable ($p < 0.05$) reduction in the percentage of tubules with positive TDI and SPI and a decreased Johnsen' score were revealed in the VCL-induced group (Fig. 2G, 2H, 2I).

VCL Diminished Testicular TAC and Enzymatic Antioxidant Status and Amplified the Apoptosis Index

To show the effect of VCL on testicular antioxidant status, the testicular TAC and the activities of GPX, SOD, and CAT were analyzed. The VCL-induced group showed a remarkable ($p < 0.05$) reduction in the TAC level and GPX, SOD, and CAT activities compared to the control rats (Fig. 3A–D). Based on these findings, the VCL could significantly ($p < 0.05$) suppress the testicular antioxidant status. To confirm the oxidative-induced damage and compare the subcapsular and central zones for the severity and portion of VCL-induced ROS, the 8-oxodG staining was considered. Observations showed a significant increment in the immunoreactivity of 8-oxo-dG (a marker for oxidative DNA damage) in the cross-sections of VCL-induced testicles, which was more evident in the subcapsular area. As a substantial finding, the most immunoreactivities were revealed in the seminiferous tubules located close to the varicose vessels (Fig. 4A, 4B, 4C). Simultaneously, with increased immunoreactivity of 8-oxo-dG, the apoptotic index increased in the seminiferous tubules close to the varicose vessels. Moreover, the subcapsular zone showed a higher apoptosis index than the central area (Fig. 4D, 4E, 4F).

VCL Decreased the BER Enzyme Level

The rats in the VCL-induced group exhibited a significant reduction in the mRNA levels of the UNG and MPG enzymes (Fig. 5A). However, to assess UNG and MPG's protein levels and compare the difference between sub-capsular and central zones in expressing UNG and MPG, the IHC staining was conducted. The results about cell count and software analysis showed a significant ($p < 0.05$) reduction in the UNG^+ and MPG^+ cell count/seminiferous tubule as well as pixel-based intensity/2350 μm × 2350 μm of the tissue (Fig. 5B, 5C, 5D, 5E). The tubules nearby to the varicose veins represented intensive changes.

Varicocele Enhanced p21 and Inhibited Cyclin D1/cdk4 Complex

Considering the crosstalk between the oxidative DNA damage and Cyclin D1, cdk4, and p21 expression, the distribution of Cyclin $D1^+$, $Cdk4^+$, and $p21^+$ cells in the seminiferous tubules nearby to the varicose vessels in the sub-capsular and central areas of testicular cross-section were investigated using IHC staining. Cross-sections of the VCL-induced group exhibited a remarkable ($p < 0.05$) increment in the $p21^+$ cell number/seminiferous tubule in both subcapsular and central zones, which was revealed evident in the sub-capsular area (Fig. 6A, 6B, 6C). However, the seminiferous tubules at the same regions represented a remarkable ($p < 0.05$) reduction in the numbers of $cdk4^+$

and Cyclin D1$^+$/seminiferous tubules nearby to the varicose vessels (Fig. 6D). Comparing two portions of one cross-section in the VCL-induced group revealed lower cdk4$^+$ and Cyclin D1$^+$ cells in the subcapsular zone compared to the central area. Moreover, the pixel-based intensity analysis concerning the p21, Cyclin D1, and cdk4 proteins was considered. A remarkable increment in the p21-related, as well as a significant reduction in the Cyclin D1-and cdk4-related SUM intensities, were revealed in the VCL-induced group (Fig. 6E, 6F, 6G).

Discussion

The VCL has been shown as the leading cause of male infertility. Despite a large number of scholarly articles, it still elicits debate among scientists and andrologists for almost a century. However, to date, contracted blood dynamicity and massive varicose in the testicular microvasculature as well as pampiniform plexus, due to absence and/or incomplete valve generation in the spermatic vein, have revealed explicitly in the testicular tissue of VCL patients [3, 9]. More animal model studies [16, 17, 22] and clinical demonstrations [18, 41–43] have shown multi-factorial etiology, including a significant reduction in the testicular antioxidant and endocrine statuses, as well as supra-physiologic cytokine surge in both testicles and semen. Despite all these researches, it remains to be revealed whether VCL-induced varicose homogenously affects the testicular tissue or whether the seminiferous tubules nearby dominant varicose vessels are differentially affected from those in distance. Moreover, based on this possibility, it should be illustrated that macromolecules' homoeostatic expressions/reactions are changed in the tubules nearby varicose expansion or systematically in all testicular tissue. Therefore, the molecular and biochemical alterations are investigated in the present study, albeit by more focusing on the distance of tubules from varicose vessels and comparing the changes between the sub-capsular (with more dominant varicose) and central (with the lower expansion of varicose) areas. Since we believe that the survived tubules with more distance from varicose vessels may respond to the medication and surgical interventions (varicocelectomy) more prominently.

As a preliminary and fundamental finding, the animals in the VCL-induced group showed a significant reduction in the blood velocity, reflecting the presence of dominant varicose in the left-side testicles microcirculation. In animal models and even in patients with VCL [44], because of anatomical complexity and testicular vessels' small size, it is hard to distinguish the blood velocity between sub-capsular and central areas. However, analyzing varicose as well as the vascular diameter in the histopathological slides most probably can reflect diminished blood velocity [45]. Thus, the histological cross-sections were prepared, and we found an intensive vascular dilation simultaneous with progressive varicose, which was revealed to be more evident in the sub-capsular zone. So far, in corroboration with previous studies using animal models [46] and clinical findings [47], a significant impairment in blood velocity, and as new findings, more evident changes in the sub-capsular area were revealed in the current study. Moreover, distinguished histological and molecular changes were revealed in the seminiferous tubules nearby varicose vessels, implying a positive correlation between varicose, its intensity or expansion, and the spermatogenesis failure.

As mentioned above, among different VCL-induced etiologies, oxidative stress has been highlighted due to its direct impacts on testicular germ and somatic cells as well as their lipid, protein, and RNA and DNA contents [10, 17, 19]. However, all scholarly articles have explored the oxidative stress in the testicles with VCL, regardless of analyzing the varicose vessels as primitive sources of ROS and/or the possible correlation between varicose severity and ROS amount. Therefore, to show this correlation, the immunoreactivity of 8-oxo-dG as a sensitive marker for ROS-induced DNA damages [48, 49] was investigated. The cross-sections of VCL-induced testicles exhibited a significant increment in the 8-oxo-dG immunoreactivity, mainly in seminiferous tubules nearby the varicose vessels, more prominently in the sub-capsular area. Given that the DNA adduct, 8-oxo-dG, is formed following the OH radical interaction with the DNA guanine base [49, 50], this finding most likely indicates higher ROS generation nearby varicose vessels and/or at least in the current study, which represents a possible correlation between varicose intensity and ROS amount, because the expanded microvasculature and an increased vascular diameter simultaneous with significantly higher 8-oxo-dG immunoreactivity have been revealed in the sub-capsular area. However, it should not be forgotten that the molecular protective system's capability in repairing oxidative DNA damage is as crucial as oxidative DNA damage. Although several pathways are involved in the DNA repairing system, the oxidative DNA damage is repaired primarily by the BER pathway using the mono-functional DNA glycosylases MPG and UNG [32, 51]. Moreover, it should not be forgotten that the endogenous antioxidant enzymes (GPX, SOD, and catalase) play a crucial role before and/or alongside the BER system to protect the DNA content against ROS [52]. Thus, both of these systems were analyzed by local and global investigating the BER enzyme-related changes (using IHC

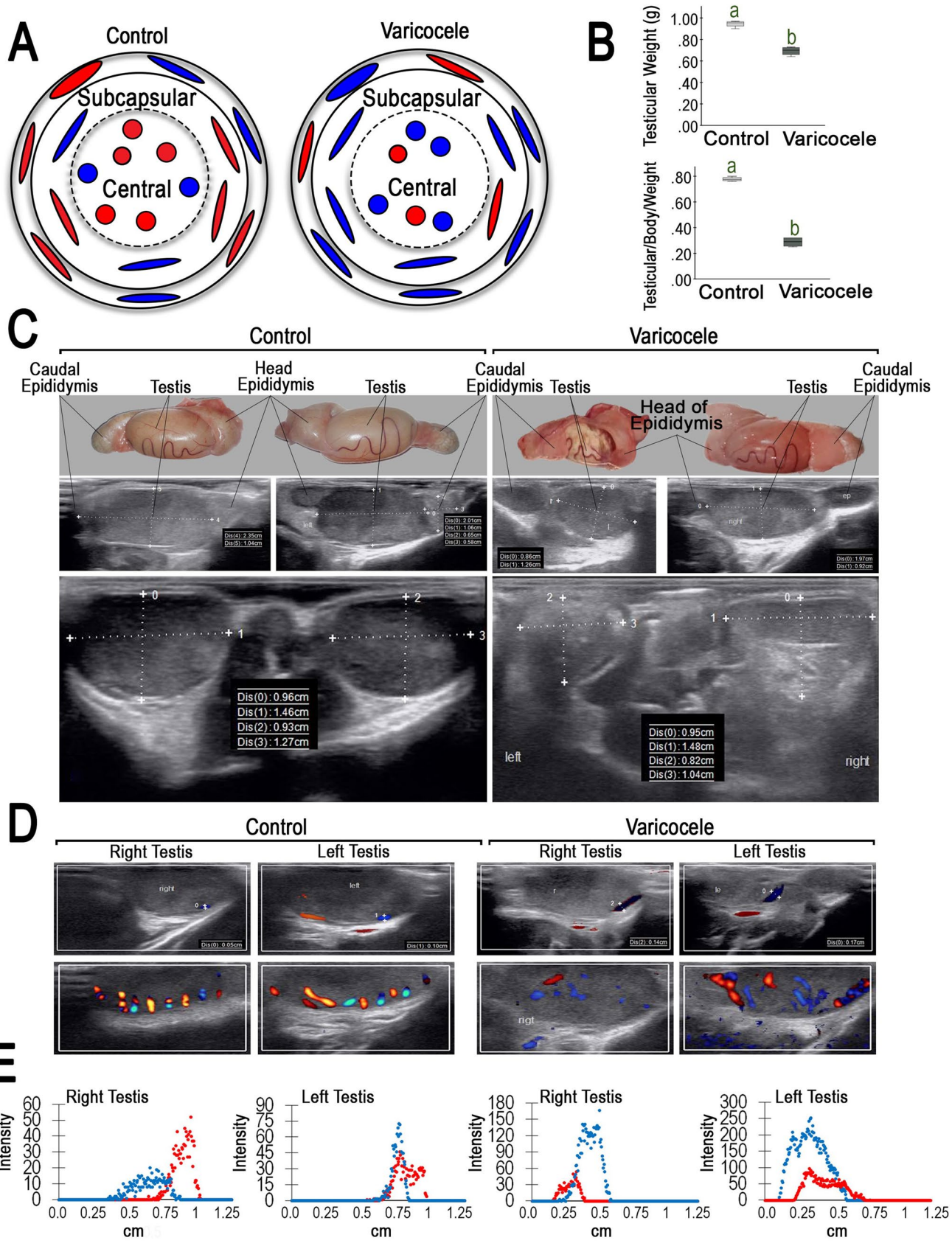
A
Control
Varicocele
Subcapsular
Central
B
Testicular Weight (g)
1.00
.80
.60
.40
.20
.00
a
b
Control
Varicocele
Testicular/Body/Weight
.80
.60
.40
.20
.00
C
Caudal Epididymis
Testis
Head Epididymis
Head of Epididymis
Dis(0):0.96cm
Dis(1):1.46cm
Dis(2):0.93cm
Dis(3):1.27cm
Dis(0):0.95cm
Dis(1):1.48cm
Dis(2):0.82cm
Dis(3):1.04cm
left
right
D
Right Testis
Left Testis
E
Intensity
cm

◂**Fig. 1** **A** Schematic photomicrograph of the testicular cross-section in a sonographic panel: varicose vessels are marked in blue, and the vessels with normal blood dynamicity are marked in red; **B** testicular and testicular/total body weight gains; **C** in comparison to the right-hand side and those from control animal, a significant reduction in the size of left-hand side testicle of varicocele (VCL)-induced rats is observable in the longitudinal ultrasonogram in the first panel as well as the magnified transverse section in the second panel; **D** Color Doppler ultrasonogram is showing a prominent increment in the vessel size and number in the left-hand side testicle of VCL-induced rat; and **E** software analyses of red (artery) and blue colors (vein) in both right and left-side testicles in both control and VCL-induced rats

and qRT-PCR) and evaluating global testicular GPX, SOD, and catalase activities along with the testicular TAC level. A remarkable reduction in the mRNA levels of MPG and UNG was revealed in VCL-induced groups. Moreover, the seminiferous tubules nearby the varicose vessels exhibited a significant reduction in MPG^+ and UNG^+ cell distribution than those with more distance, suggesting low protein expression of these enzymes close to the expanded varicose. At the same time, the global TAC, GPX, SOD, and catalase levels decreased in the VCL-induced testicles representing a significant failure in the antioxidant defense system. Indeed, the supra-physiologic generation of ROS in the VCL condition has been shown to suppress the antioxidant status of testicular tissue [42, 53], while here we found that, in addition to failed global testicular antioxidant status, the BER intermediated repairing system is significantly suppressed, which in turn can intensify the ROS-induced DNA damage in the

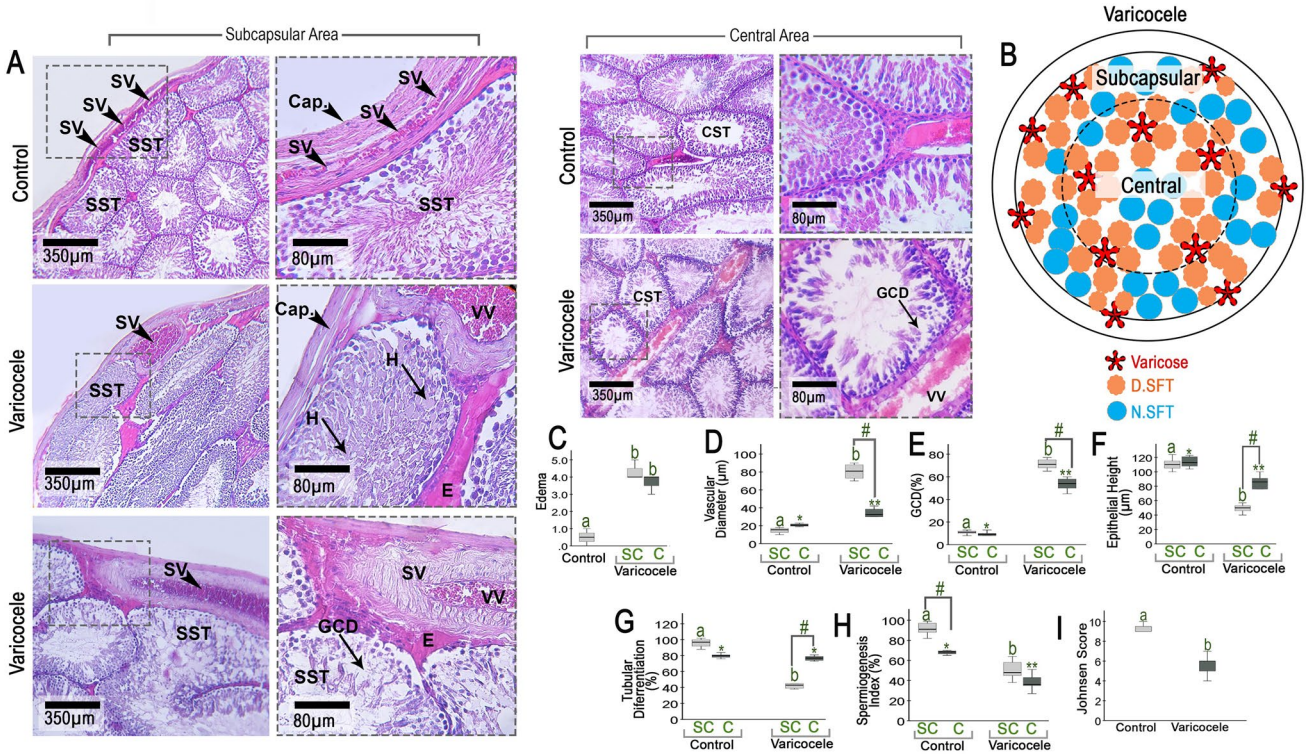

Fig. 2 **A** Cross-sections of testicular tissue in control and varicocele (VCL)-induced groups: note capsule (Cap), intact subcapsular vessels (SV), and seminiferous tubules in the subcapsular area (SST) in the control group, which are significantly changed in the VCL-induced group. See massive varicose vessels (VV), edema €, germ cell dissociation (GCD), and hyalinization (H) of germ cells in the seminiferous tubules of the subcapsular area in the cross-sections from VCL-induced rat. The cross-section from the VCL-induced group exhibits varicose vessel (VV) and massive germ cell dissociation in the tubule nearby the varicose vessels in the central zone, H&E staining; **B** schematic view of testicular cross-section; representing the varicose vessels, damaged (D. SF) and normal seminiferous tubules, **C** interstitial tissue edema (0: no edema; 1: faint edema; 2: moderate edema; 3: moderate edema; 4: moderate to severe; 5: severe edema), **D** vascular diameter, **E** percentage of seminiferous tubules with germinal cell dissociation, **F** germinal epithelium height, **G** seminiferous tubules diameter, **H** percentage of seminiferous tubules with positive spermiogenesis index, and **I** Johnsen's score; all data are presented in mean ± SD, ($n = 15$/each group). Letters are presenting statistically significant ($p < 0.05$) differences between subcapsular (SC) areas of control and VCL groups; * and ** are presenting the significant differences ($p < 0.05$) between central zones of control and VCL group, and # is presenting significant differences ($p < 0.05$) between subcapsular and central zones in each group

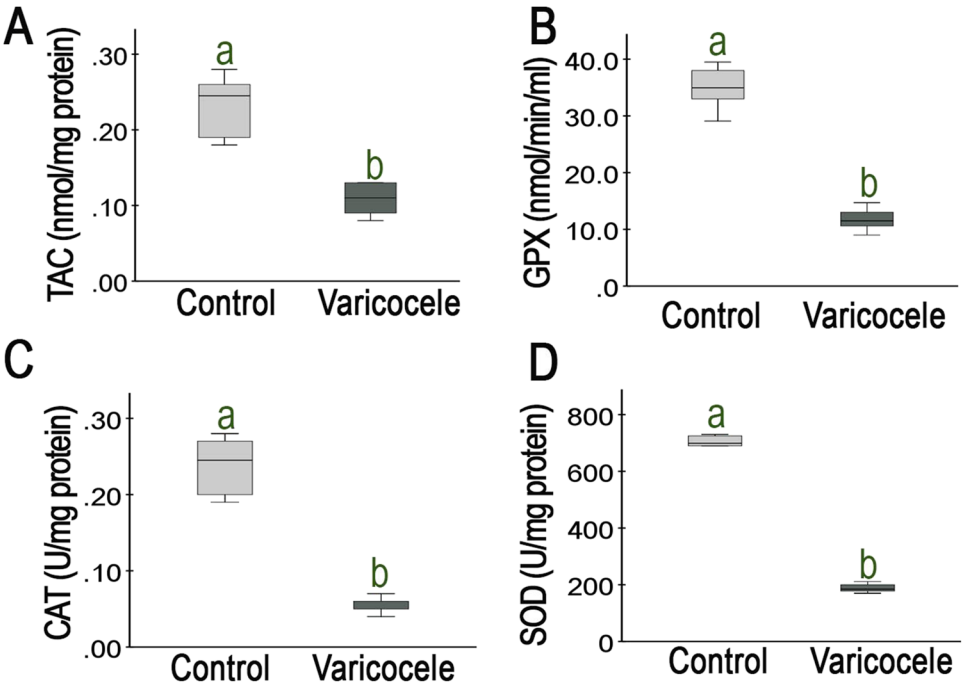

Fig. 3 **A** Testicular total antioxidant (TAC), **B** glutathione peroxidase (GPX), (**C**) catalase, (**D**) superoxide dismutase (SOD) in control and varicocele groups; all data are presented in mean ± SD, ($n = 15$/each group). Letters are presenting statistically significant ($p < 0.05$) differences between control and varicocele groups

testicular cellularity. Concerning the BER pathway's role in repairing the oxidative DNA damage as well as minimizing the number of potential mutations on DNA after oxidative damage [54–56], we can suggest that VCL by suppressing the UNG and MPG glycosylases expression can boost the nucleophilic DNA bases oxidation leading to base loss and/or strand breaks. In line with this suggestion, as mentioned above, we found an increased 8-oxo-dG reactivity representing guanine oxidation as well as elevated late apoptotic cells, exhibiting VCL-induced DNA strand break. Moreover, given the symmetry of decreased BER enzyme expression and an explicit increment in the DNA damage (marked by TUNEL), mainly in the tubes nearby varicose vessels, these vessels seem to be one of the most important causes of BER system failure. They can also intensify the ROS-related damages due to low blood dynamicity and velocity, leading to failed exportation of the ROS and toxic defecations produced by the damaged cells.

However, any DNA damage, regardless of the underlying cause(s), activates the proliferative germ cells' cycle control system [28, 29]. Among several proteins controlling this system, the p21, as a potent Cyclin-dependent kinase inhibitor (CKI), plays a vital role in stopping the cell cycle stages in mitotic G1 to S phases [23]. Following DNA damage, the p21 interacts with cdk4 and stops the Cyclin D1/cdk4 complex formation from holding the cycle development. Inline, it initiates the DNA repairing machinery and/or p53-dependent apoptosis pathway [29, 43]. The VCL-induced rats exhibited a remarkable increment in p21 expression, prominently in the seminiferous tubules nearby the varicose vessels. More intensive reactions were revealed in the tubules located in the sub-capsular area, which were presenting higher apoptotic cells simultaneous with p21 overexpression. In contrast, a significant reduction in the Cyclin $D1^+$ and cdk-4^+ was revealed in the same tubules. Given the increased apoptosis in the tubules exhibiting an elevated expression of p21 and the symmetry of this situation with an expanded varicose, we can conclude that a remarkable increment in the p21 expression might boost the p53-dependent apoptosis more intensively in the tubules nearby varicose vessels. Since, Cyclin D1/cdk4 complex plays a crucial role in cell cycle progression, and considering the pro-inhibitory role of p21 in Cyclin D1/cdk4 complex formation, it can be suggested that a diminished expression of Cyclin D1 and cdk4 simultaneous with p21/cdk4 over interaction could significantly suppress the spermatogenesis, mainly in tubules nearby the varicose vessels and much more evident in the sub-capsular area compared to the central portion.

Conclusion

The present study showed that, at least in rat models, the severity and expansion of varicose vessels in the sub-capsular area are higher compared to the central area. Moreover, the oxidative stress-associated histological and molecular changes are more prominently detectable in the seminiferous tubules nearby the varicose vessels. Accordingly, the tubules nearby the varicose vessels represent significantly higher oxidative DNA damage and p21 as well as lower

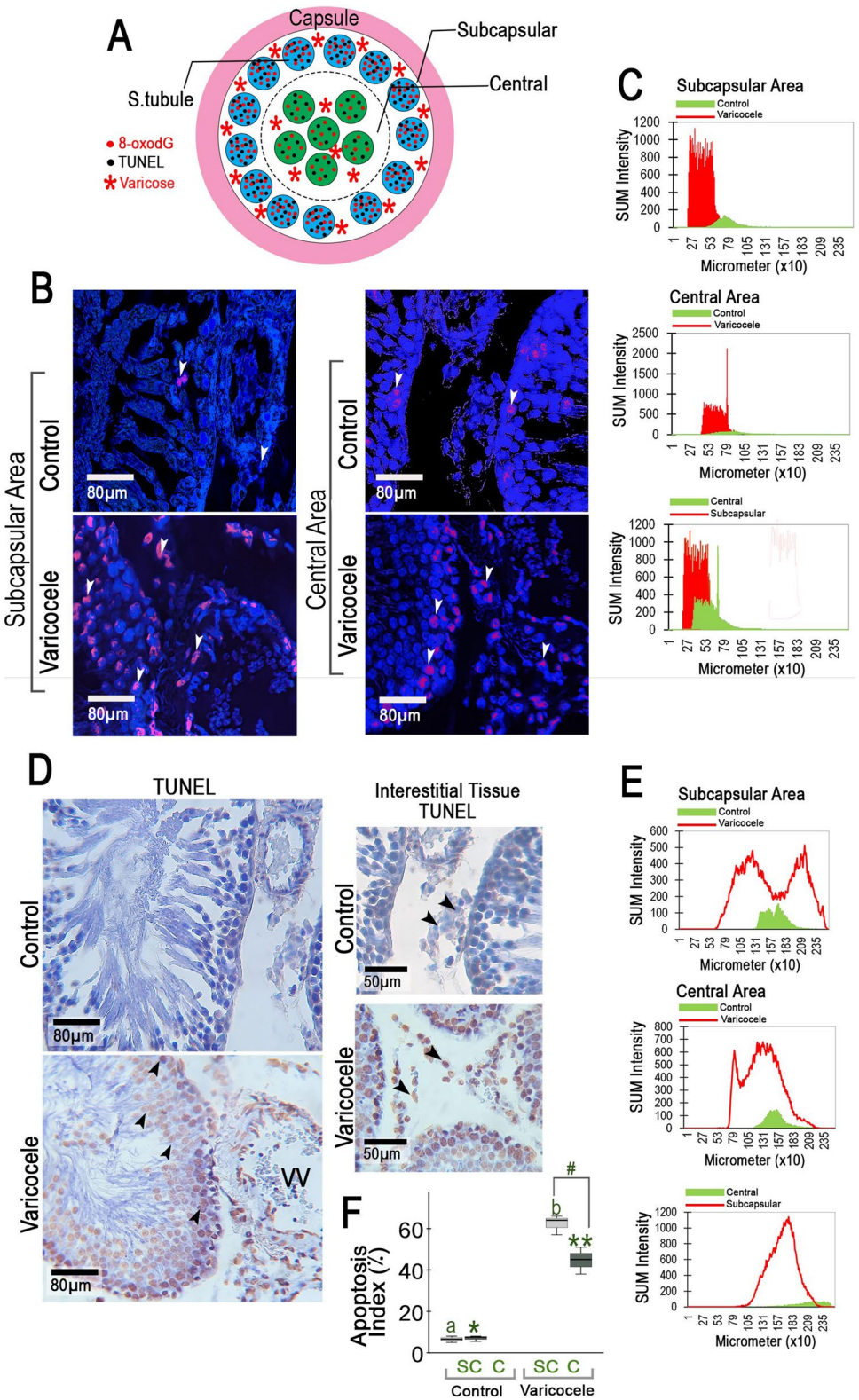

Fig. 4 **A** Schematic photomicrograph of a testicular cross-section from varicocele (VCL) group: positive immunoreactions for 8-oxodG and apoptotic cells are presented in green and black spots, respectively. The seminiferous tubules close to varicose vessels are presenting massive 8-oxodG^{+} and apoptotic spots. The tubules located in the subcapsular area are presenting higher positive spots versus those in the central zone; **B** immunofluorescent staining of 8-oxo-dG: the positive reactions are shown with arrowheads; **C** software analysis for red fluorescent-stained pixels/total pixels in 2350 × 2350 µm of tissue, representing positive 8-oxodG immunoreactivity. Note an increased 8-oxo-dG immunoreactivity in both subcapsular and central zones in the varicocele group compared to the cross-sections of the control group; **D** TUNEL staining: note an increased population of apoptotic germ and somatic cells (head arrows) nearby varicose vessel (VV) in the varicocele group, €; **E** software analysis for brown-stained pixels/total pixels in 2350 × 2350 µm of tissue, representing apoptotic cells; **F** mean apoptosis index in different groups, all data are presented in mean ± SD, ($n = 15$/each group). Letters are presenting statistically significant ($p < 0.05$) differences between subcapsular (SC) areas of control and VCL groups; * and ** are presenting the significant differences ($p < 0.05$) between central zones of control and VCL group, and # is presenting significant differences ($p < 0.05$) between subcapsular and central zones in each group

Cyclin D1 and cdk4 expression compared to those tubules with more distance. Based on these findings, we suggest that in a long-term VCL condition, there might be much more hope to see the ameliorative effects of antioxidant and/or surgical therapies in the central portion, because we suppose that the varicose vessels, due to their inability to appropriate

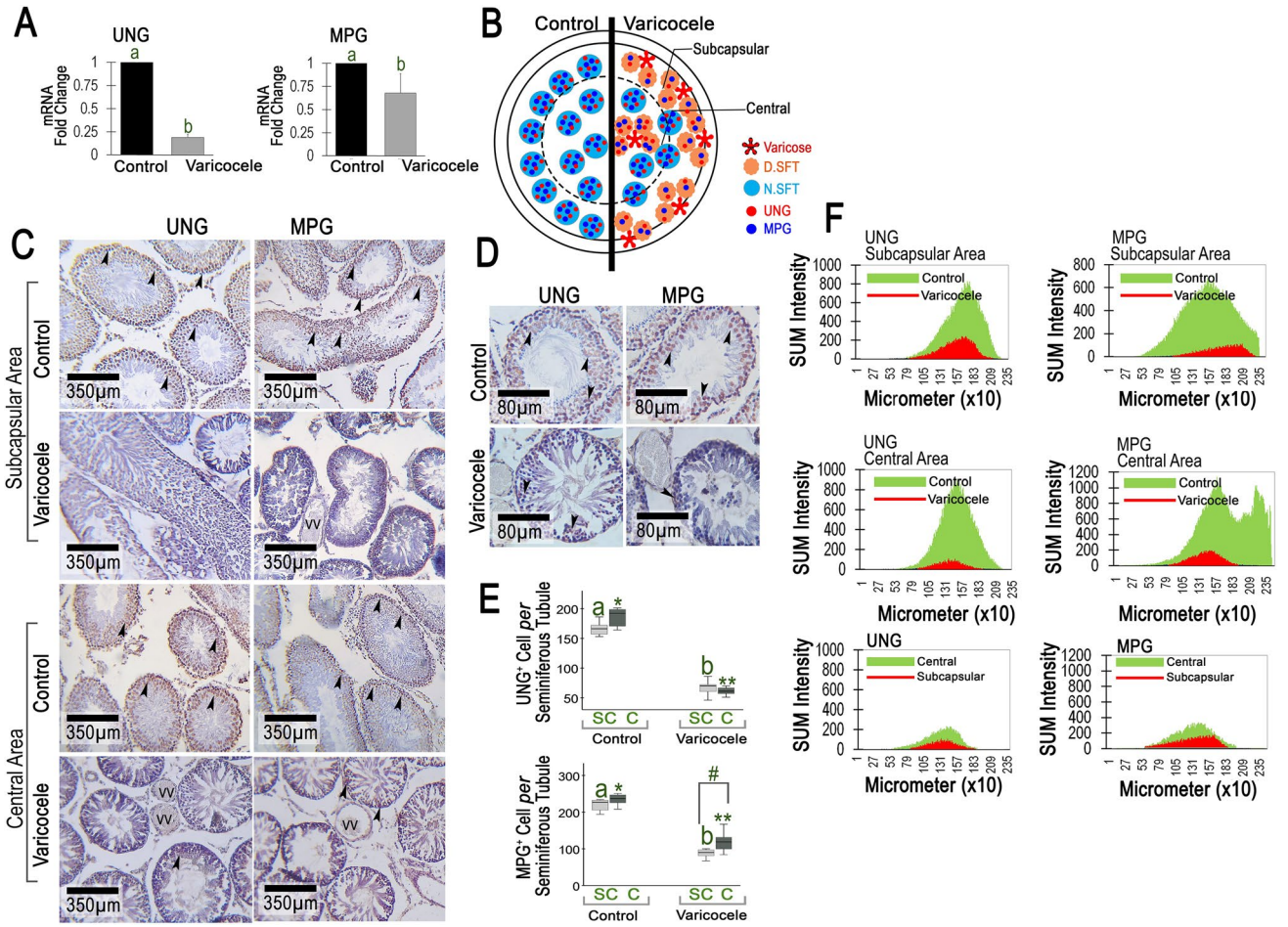

Fig. 5 **A** mRNA levels of uracil-DNA glycosylase (UNG) and methylpurine DNA glycosylase (MPG) in different groups; **B** schematic photomicrograph representing a decreased distribution of UNG^+ and MPG^+ cells in the damaged seminiferous tubules nearby varicose vessels, more evidently in the subcapsular area; **C** cross-sections of seminiferous tubules (UNG and MPG immunohistochemical staining): See decreased UNG^+ and MPG^+ cells in the tubules (head arrows) nearby the varicose vessels (VV) in both subcapsular and central zones of the varicocele (VCL)-induced group; **D** higher magnifications of seminiferous tubules: see varicose vessels in the varicocele group and higher numbers of UNG^+ and MPG^+ cells in the tubules from control group; **E** mean numbers of UNG^+ and MPG^+ cells per one seminiferous tubule with same criteria; **F** software analysis for brown-stained pixels/total pixels in 2350 × 2350 µm of tissue, representing positive UNG and MPG-stained cells. The graphs are representing lower reactivity in both subcapsular and central zones of VCL-induced group, which is more prominent in the subcapsular area. All data are presented in mean ± SD, ($n = 15$/each group). Section A: Letters are presenting statistically significant ($p < 0.05$) differences between control and varicocele groups; Section E: Letters are presenting statistically significant ($p < 0.05$) differences between subcapsular (SC) areas of control and VCL groups; * and ** are presenting the significant differences ($p < 0.05$) between central zones of control and VCL group

exportation of oxidants and defecations, are the main source of ROS generation and effectiveness.

Study Limitations and Clinical Applications

The current study is shedding a new light into testicular histopathology evaluation post VCL-induction in rat models, however, using stereological histopathology method may improve the findings. Moreover, evaluating more DNA repairmen involved enzymes, including nucleotide excision repair (NER)–associated enzymes, can improve our understanding of the DNA repair mechanisms in testis during VCL-induced condition. Additionally, evaluating these enzymes alterations post-VCL therapy, whether varicocelectomy or medical therapy, may elucidate more clinical expected outcomes. As the clinical application, we should mention that the current study is providing a new

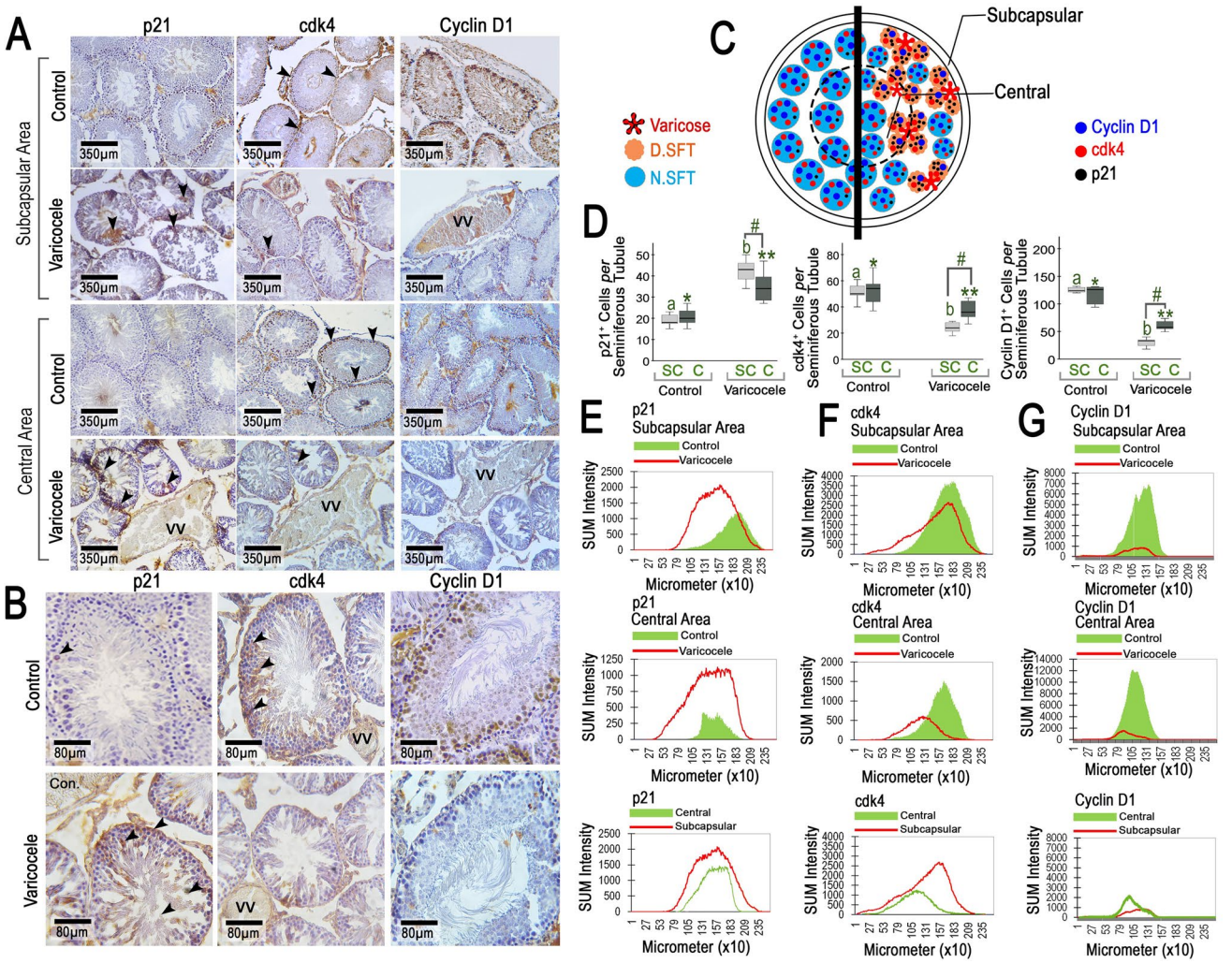

Fig. 6 **A** Cross-sections of seminiferous tubules (p21, Cyclin D1, and cdk4 immunohistochemical staining): see increased $p21^+$ and decreased Cyclin $D1^+$ and $cdk4^+$ cells in the tubules (head arrows) nearby the varicose vessels (VV) in both subcapsular and central zones of the varicocele (VCL)-induced group; **B** higher magnifications of seminiferous tubules: see varicose vessels (VV) and lower numbers of $p21^+$, Cyclin $D1^+$, and $cdk4^+$ cells in the tubules from varicocele group; **C** schematic photomicrograph representing a decreased distribution of Cyclin $D1^+$ and $cdk4^+$ as well as increased $p21^+$ cells in the damaged seminiferous tubules nearby varicose vessels, more evidently in the subcapsular area; **D** mean numbers of $p21^+$, Cyclin $D1^+$, and $cdk4^+$ cells *per* one seminiferous tubule with same criteria. Software analysis for brown-stained pixels/total pixels in 2350 × 2350 μm of tissue, representing positive **E** p21, **F** cdk4, and **G** Cyclin D1 stained cells. Letters are presenting statistically significant ($p < 0.05$) differences between subcapsular (SC) areas of control and VCL groups; * and ** are presenting the significant differences ($p < 0.05$) between central zones of control and VCL group, and # is presenting significant differences ($p < 0.05$) between subcapsular and central zones in each group

foundation for expected area to observe primary recovery portion in testis post varicocelectomy. Moreover, in case of non-obstructive azoospermia patients, in which the varicocelectomy surgery is not an option according to 2020 AUA/ASRM guideline, and assisted reproductive technology (ART) based on testicular sperm extraction (TESE) is the treatment approach. Thus, the current study and furthermore studies in line may provide a new approach based on testis vascular positions to increase the chance of retrieving high quality sperms from VCL patient's testicular tissue.

Acknowledgements The authors would like to thank the Department of histology and embryology, the Department of Surgery and Imaging, the Faculty of Veterinary medicine, Urmia University, and Department of Animal Biotechnology, Jahad Daneshgahi Biotechnology Research Institute, Royan Research Institute of Reproductive Medical Research Center, Isfahan, Iran, for financial and technical support. Moreover, the authors wish to thank RASTA Specialized Research Institute (RSRI) for laboratory and technical assists. This manuscript is a part of Aram Minas's Doctorate of Veterinary thesis Number; 1717, approved by the scientific deputy of Urmia University. In addition, we thank The Sao Paulo Research Foundation for the scholarship of Aram Minas (number: 2021/09149-3).

Author Contribution Aram Minas: laboratory analyses, manuscript draft; Mazdak Razi: study design, laboratory and statistical analyses, data presentation, writing the manuscript; Mohammad Hossein Nasr-Esfahani: study design, laboratory analyses, manuscript edition; Seyed Mohammad Hashemi-Asl: sonography and laboratory analyses, Marzyeh Tavalaee: study design. It should be noted that all the authors read and approved the submitted version of the study.

Data Availability The datasets of the current study can be available by the corresponding author upon reasonable request.

Declarations

Ethics Approval All experimental protocols were evaluated and approved by the Faculty of Veterinary medicine's ethical committee, Urmia University (Ethical Number: IR-UU-AEC-1779/DA/3).

Consent for Publication The authors approved the submitted version of study for publication.

Conflict of Interest The authors declare no competing interests.

References

1. Sharlip ID, Jarow JP, Belker AM, Lipshultz LI, Sigman M, Thomas AJ, Schlegel PN, Howards SS, Nehra A, Damewood MD, Overstreet JW, Sadovsky R. Best practice policies for male infertility. Fertil Steril. 2002;77:873–82.
2. Dabaja AA, Schlegel PN. Medical treatment of male infertility. Transl Androl Urol. 2014;3:9–16.
3. Razi M, Malekinejad H. Varicocele-induced infertility in animal models. Int J Fertil Steril. 2015;9:141–9.
4. Baker HWG. Male Infertility. Endocrinol Metab Clin North Am. 1994;23:783–93.
5. Kamal KM, Jarvi K, Zini A. Microsurgical varicocelectomy in the era of assisted reproductive technology: influence of initial semen quality on pregnancy rates. Fertil Steril. 2001;75:1013–6.
6. Lorenc T, Krupniewski L, Palczewski P, Gołębiowski M. The value of ultrasonography in the diagnosis of varicocele. J Ultrason. 2016;16:359–70.
7. Braedel HU, Steffens J, Ziegler M, Polsky MS, Platt ML. A possible ontogenic etiology for idiopathic left varicocele. J Urol. 1994;151:62–6.
8. Fretz PC, Sandlow JI. Varicocele: current concepts in pathophysiology, diagnosis, and treatment. Urol Clin North Am. 2002;29:921–37.
9. Sofikitis N, Dritsas K, Miyagawa I, Koutselinis A. Anatomical characteristics of the left testicular venous system in man. Arch Androl. 1993;30:79–85.
10. Salmani S, Razi M, Sarrafzadeh-Rezaei F, Mahmoudian A. Testosterone amplifies HSP70-2a, HSP90 and PCNA expression in experimental varicocele condition: implication for DNA fragmentation. Reprod Biol. 2020;20:384–95.
11. Shiraishi K, Takihara H, Matsuyama H. Elevated scrotal temperature, but not varicocele grade, reflects testicular oxidative stress-mediated apoptosis. World J Urol. 2010;28:359–64.
12. Dada R, Shamsi MB, Venkatesh S, Gupta NP, Kumar R. Attenuation of oxidative stress & DNA damage in varicocelectomy: implications in infertility management. Indian J Med Res. 2010;132:728–30.
13. Romeo C, Ientile R, Impellizzeri P, Turiaco N, Teletta M, Antonuccio P, Basile M, Gentile C. Preliminary report on nitric oxide-mediated oxidative damage in adolescent varicocele. Hum Reprod Oxf Engl. 2003;18:26–9.
14. Hassani-Bafrani H, Najaran H, Razi M, Rashtbari H. Berberine ameliorates experimental varicocele-induced damages at testis and sperm levels; evidences for oxidative stress and inflammation. Andrologia. 2019;51:e13179.
15. Hosseini M, Shaygannia E, Rahmani M, Eskandari A, Golsefid AA, Tavalaee M, Gharagozloo P, Drevet JR, Nasr-Esfahani MH. Endoplasmic reticulum stress (ER stress) and unfolded protein response (UPR) occur in a rat varicocele testis model. Oxid Med Cell Longev. 2020;2020:1–11.
16. Mazhari S, Razi M, Sadrkhanlou R. Silymarin and celecoxib ameliorate experimental varicocele-induced pathogenesis: evidences for oxidative stress and inflammation inhibition. Int Urol Nephrol. 2018;50:1039–52.
17. Khosravanian N, Razi M, Farokhi F, Khosravanian H. Testosterone and vitamin E administration up-regulated varicocele-reduced Hsp70-2 protein expression and ameliorated biochemical alterations. J Assist Reprod Genet. 2014;31:341–54.
18. Agarwal A, Prabakaran S, Allamaneni SS. Relationship between oxidative stress, varicocele and infertility: a meta-analysis. Reprod Biomed Online. 2006;12:630–3.
19. Rashtbari H, Razi M, Hassani-Bafrani H, Najaran H. Berberine reinforces Sertoli cells niche and accelerates spermatogonial stem cells renewal in experimentally-induced varicocele condition in rats. Phytomedicine. 2018;40:68–78.
20. Blumer CG, Restelli AE, Giudice PTD, Soler TB, Fraietta R, Nichi M, Bertolla RP, Cedenho AP. Effect of varicocele on sperm function and semen oxidative stress: varicocele, sperm function and oxidative stress. BJU Int. 2012;109:259–65.
21. Gholirad S, Razi M, Hassani Bafrani H. Tracing of zinc and iron in experimentally induced varicocele: correlation with oxidative, nitrosative and carbonyl stress. Andrologia. 2017;49:e12687.
22. Razi M, Sadrkhanloo R-A, Malekinejad H, Sarafzadeh-Rezaei F. Varicocele time-dependently affects DNA integrity of sperm cells: evidence for lower in vitro fertilization rate in varicocele-positive rats. Int J Fertil Steril. 2011;5:174–85.
23. Zamir-Nasta T, Razi M, Shapour H, Malekinejad H. Roles of p21, p53, cyclin D1, CDK-4, estrogen receptor α in aflatoxin B1-induced cytotoxicity in testicular tissue of mice. Environ Toxicol. 2018;33:385–95.
24. Wang W, Heideman L, Chung CS, Pelling JC, Koehler KJ, Birt DF. Cell-cycle arrest at G2/M and growth inhibition by apigenin in human colon carcinoma cell lines. Mol Carcinog. 2000;28:102–10.
25. Quelle DE, Ashmun RA, Shurtleff SA, Kato JY, Bar-Sagi D, Roussel MF, Sherr CJ. Overexpression of mouse D-type cyclins accelerates G1 phase in rodent fibroblasts. Genes Dev. 1993;7:1559–71.
26. Wang J, Chenivesse X, Henglein B, Bréchot C. Hepatitis B virus integration in a cyclin A gene in a hepatocellular carcinoma. Nat. 1990;343:555–7.
27. Hagen KR, Zeng X, Lee M-Y, Tucker Kahn S, Harrison Pitner MK, Zaky SS, Liu Y, O'Regan RM, Deng X, Saavedra HI. Silencing CDK4 radiosensitizes breast cancer cells by promoting apoptosis. Cell Div. 2013;8:10.
28. Cheraghi S, Razi M, Malekinejad H. Involvement of cyclin D1 and E2f1 in zearalenone-induced DNA damage in testis of rats. Toxicon Off J Int Soc Toxinology. 2015;106:108–16.
29. Amin M, Razi M, Sarrafzadeh-Rezaei F, Shalizar Jalali A, Najafi G. Berberine inhibits experimental varicocele-induced cell cycle arrest via regulating cyclin D1, cdk4 and p21 proteins expression in rat testicles. Andrologia. 2018;50(4):e12984. https://doi.org/10.1111/and.12984.

30. Liu W, Bi X, Tocco G, Baudry M, Schreiber SS. Increased expression of cyclin D1 in the adult rat brain following kainic acid treatment. Neuroreport. 1996;7:2785–9.
31. Krokan HE, Bjørås M. Base excision repair. Cold Spring Harb Perspect Biol. 2013;5:a012583.
32. Iyama T, Wilson DM. DNA repair mechanisms in dividing and non-dividing cells. DNA Repair. 2013;12:620–36.
33. Lindahl T. Instability and decay of the primary structure of DNA. Nat. 1993;362:709–15.
34. Likhite VS, Cass EI, Anderson SD, Yates JR, Nardulli AM. Interaction of estrogen receptor alpha with 3-methyladenine DNA glycosylase modulates transcription and DNA repair. J Biol Chem. 2004;279:16875–82.
35. Rezaei-Agdam H, Moshari S, Nahari E, Minas A, Daliri Z, Hallaj M, Razi M. Zeta and hyaluronic acid assessments, novel sperm selection procedures, in animal model for male infertility. Andrologia. 2019;51:e13447.
36. Horecka A, Biernacka J, Hordyjewska A, Dąbrowski W, Terlecki P, Zubilewicz T, Musik I, Kurzepa J. Antioxidative mechanism in the course of varicose veins. Phlebology. 2018;33:464–9.
37. Turner TT. The study of varicocele through the use of animal models. Hum Reprod Update. 2001;7:78–84.
38. Kwon JW, Kim WS, Cheon J-E, Kim CJ, Kim I-O, Yeon KM. Evaluation of testicular viability by power Doppler ultrasonography in experimentally induced acute testicular torsion. Invest Radiol. 2005;40:682–7.
39. Lowry OH, Rosebrough NJ, Farr AL, Randall RJ. Protein measurement with the Folin phenol reagent. J Biol Chem. 1951;193:265–75.
40. Minas A, Najafi G, Shalizar Jalali A, Razi M. Fennel induces cytotoxic effects against testicular germ cells in mice; evidences for suppressed pre-implantation embryo development. Environ Toxicol. 2018;33(8):841-850. https://doi.org/10.1002/tox.22570.
41. Mostafa T, Rashed LA, Nabil NI, Osman I, Mostafa R, Farag M. Seminal miRNA relationship with apoptotic markers and oxidative stress in infertile men with varicocele *BioMed Res*. Int. 2016;2016:4302754.
42. Abdel-Meguid TA, Farsi HM, Al-Sayyad A, Tayib A, Mosli HA, Halawani AH. Effects of varicocele on serum testosterone and changes of testosterone after varicocelectomy: a prospective controlled study. Urol. 2014;84:1081–7.
43. Zeinali M, Hadian Amree A, Khorramdelazad H, Karami H, Abedinzadeh M. Inflammatory and anti-inflammatory cytokines in the seminal plasma of infertile men suffering from varicocele. Andrologia. 2017;49(6). https://doi.org/10.1111/and.12685.
44. Tarhan S, Gümüs B, Gündüz I, Ayyildiz V, Göktan C. Effect of varicocele on testicular artery blood flow in men–color Doppler investigation. Scand J Urol Nephrol. 2003;37:38–42.
45. Sobhy N, El-Mulla K, Elmessiry M, El-Gendi S. Histopathological and immunohistochemical study of the wall of spermatic veins and its potential role in the development of varicocele testis. Alex J Med. 2011;47:209–15.
46. Tian RH, Ma M, Zhu Y, Yang S, Wang ZQ, Zhang ZS, Wan CF, Li P, Liu YF, Wang JL, Liu Y, Yang H, Zhang ZZ, Liu LH, Gong YH, Li FH, Hu HL, He ZP, Huang YR, Li Z. Effects of aescin on testicular repairment in rats with experimentally induced varicocele. Andrologia. 2014;46:504–12.
47. ur Rehman K, Qureshi AB, Numan A, Zaneb H, Yousaf MS, Rabbani I, Rehman H. Pressure flow pattern of varicocele veins and its correlation with testicular blood flow and semen parameters. Andrologia. 2018;50(2). https://doi.org/10.1111/and.12856.
48. Haghdoost S, Czene S, Näslund I, Skog S, Harms-Ringdahl M. Extracellular 8-oxo-dG as a sensitive parameter for oxidative stress in vivo and in vitro. Free Radic Res. 2005;39:153–62.
49. Ock C-Y, Kim E-H, Choi DJ, Lee HJ, Hahm K-B, Chung MH. 8-Hydroxydeoxyguanosine: not mere biomarker for oxidative stress, but remedy for oxidative stress-implicated gastrointestinal diseases. World J Gastroenterol. 2012;18:302–8.
50. Sheridan J, Wang L-M, Tosetto M, Sheahan K, Hyland J, Fennelly D, O'Donoghue D, Mulcahy H, O'Sullivan J. Nuclear oxidative damage correlates with poor survival in colorectal cancer. Br J Cancer. 2009;100:381–8.
51. Gunes S, Al-Sadaan M, Agarwal A. Spermatogenesis, DNA damage and DNA repair mechanisms in male infertility. Reprod Biomed Online. 2015;31:309–19.
52. van Houten-Schat MA, Berkhout JJ, van Dijk N, Endedijk MD, Jaarsma ADC, Diemers AD. Self-regulated learning in the clinical context: a systematic review. Med Educ. 2018;52:1008–15.
53. Lorian K, Kadkhodaee M, Kianian F, Abdi A, Ranjbaran M, Ashabi G, Seifi B. Long-term NaHS administration reduces oxidative stress and apoptosis in a rat model of left-side varicocele. Andrologia. 2020;52:e13496.
54. Olsen A-K, Lindeman B, Wiger R, Duale N, Brunborg G. How do male germ cells handle DNA damage? Toxicol Appl Pharmacol. 2005;207:521–31.
55. Paul C, Nagano M, Robaire B. Aging results in differential regulation of DNA repair pathways in pachytene spermatocytes in the Brown Norway rat. Biol Reprod. 2011;85:1269–78.
56. Vodicka P, Urbanova M, Makovicky P, Tomasova K, Kroupa M, Stetina R, Opattova A, Kostovcikova K, Siskova A, Schneiderova M, Vymetalkova V, Vodickova L. Oxidative damage in sporadic colorectal cancer: molecular mapping of base excision repair glycosylases in colorectal cancer patients. Int J Mol Sci. 2020;21:2473.